Growth of high quality single crystals of strontium doped (Nd,Pr)-nickelates, $Nd_{2-x}Sr_xNiO_{4+\delta}$ and $Pr_{2-x}Sr_xNiO_{4+\delta}$

Olivia Wahyudi, Monica Ceretti, Isabelle Weill, Alain Cousson, François Weill, Martin Meven, Marc Guerre, Antoine Villesuzanne, Jean-Marc. Bassat, Werner Paulus

Growth of high quality single crystals of strontium doped (Nd,Pr)-nickelates, $Nd_{2-x}Sr_xNiO_{4+\delta}$ and $Pr_{2-x}Sr_xNiO_{4+\delta}$

O. Wahyudi,‡[abcd] M. Ceretti,*[a] I. Weill,[bc] A. Cousson,[e] F. Weill,[bc] M. Meven,[f] M. Guerre,[a] A. Villesuzanne,[bcg] J.-M. Bassat[bc] and W. Paulus[a]

[a] *Institut Charles Gerhardt Montpellier, UMR 5253 CNRS-Université de Montpellier, Chimie et Cristallochimie des Matériaux, Place Eugene Bataillon, 34095 Montpellier, France*
[b] *CNRS, ICMCB, UPR 9048, F-33600 Pessac, France*
[c] *Univ. Bordeaux, ICMCB, UPR 9048, F-33600 Pessac, France*
[d] *Sciences Chimiques de Rennes, Université de Rennes 1, France*
[e] *Laboratoire Léon Brillouin, UMR 12 CEA-CNRS, Gif sur Yvette, 91191 France*
[f] *Heinz Maier-Leibnitz Zentrum (MLZ), Technische Universität München and RWTH Aachen University, Institut für Kristallographie, Outstation at MLZ, 85747 Garching, Germany*
[g] *IREET, University of Bolton, Bolton, BL3 5AB UK*

*** Corresponding authors** / E-mail: **monica.ceretti@univ-montp2.fr**

Footnotes :
† Electronic supplementary information (ESI) available: Figure S1 shows a characteristic XRD pattern of $Pr_2NiO_{4+\delta}$ after air heating at 1000 °C evidencing its partial decomposition. Figure S2 reports the X-ray diffraction patterns of crushed as-grown PSNO single crystals. Diffraction patterns obtained by XRD of the as-grown NNO single crystal, before and after annealing at 430 °C, are reported in Fig. S3. The atomic percentage of neodymium and nickel, as well as the Nd(Pr)/Ni ratio, distribution over a cross section of the as-grown NNO and PNO single crystals is depicted in Fig. S4. See DOI: 10.1039/c5ce00906e
‡ Present address: Shanghai Institute of Ceramics, Chinese Academy of Sciences, 1295 Dingxi Road, Shanghai, PR China 200050.

Abstract: Large size and high quality single crystals of $Nd_{2-x}Sr_xNiO_{4+\delta}$ and $Pr_{2-x}Sr_xNiO_{4+\delta}$, with selected composition (x = 0.0, 0.1 and 0.5), were grown by a floating-zone technique using an image furnace. We found that even small deviations from the ideal cation stoichiometry led to either NiO segregation or formation of Ni-poor $Pr_4Ni_3O_{10-x}$, or RE_xO_y intergrowth phases, rendering the title compounds unstable even under ambient conditions. Related to potential applications as membranes in SOFC, we importantly found $Nd_{2-x}Sr_xNiO_{4+\delta}$ and $Pr_{2-x}Sr_xNiO_{4+\delta}$ powders, obtained from ground stoichiometric single crystals, to be stable in air at high temperature (1000 °C), contrary to the partial decomposition observed when synthesized as polycrystalline powders by classical solid state synthesis. The presence of NiO/$Pr_4Ni_3O_{10-x}$ or RE_xO_y intergrowth phases are discussed as a drawback limiting high temperature stability for $Pr_2NiO_{4+\delta}$. Grown single crystals were characterised by neutron and X-ray diffraction as well as by electron microscopy (SEM/EDS), revealing their excellent quality in terms of composition, homogeneity and crystallinity. For each crystal, the oxygen content was determined by thermogravimetric analysis in a reductive atmosphere. Transmission electron microscopy highlighted a complex incommensurate structure for $Pr_2NiO_{4.25}$ and $Nd_2NiO_{4.25}$ with a 2D modulation vector related to oxygen ordering.

Introduction

$Nd_2NiO_{4+\delta}$ and $Pr_2NiO_{4+\delta}$ belong to the K_2NiF_4-type structure and can accommodate extra oxygen atoms on interstitial lattice sites. Their non-stoichiometry range amounts to $0 < \delta < 0.25$, showing a complex phase diagram as a function of the oxygen content δ,[1–5] which for various compounds has been reported to show charge and/or orbital ordering on a large scale.[6,7] They also exhibit an impressive capacity for oxygen ion transport down to moderate temperatures,[8] promoting them to be among the most promising candidates today for oxygen membranes or electrodes in solid oxide fuel

cells (SOFCs) as well as solid oxide electrolysis cell (SOEC) devices.[9,10] A better fundamental understanding of their high oxygen ion mobility, already present at ambient temperature, is important to optimise this class of oxygen ion conductors. Especially, the amount δ of interstitial oxygen atoms is believed to strongly affect low-energy lattice dynamics, which plays a prominent role in the oxygen diffusion mechanism.[11–13]

In recent studies on $La_2CuO_{4.07}$, combining T-dependent single crystal neutron diffraction studies with first-principles calculations,[11] the importance of specific lattice dynamics, related to large displacements of the apical oxygen atoms, was evidenced to favour low temperature oxygen diffusion, based on a phonon assisted diffusion mechanism. Specifically, interstitial oxygen atoms seem to be the triggering component for the large displacive amplitudes of the apical oxygen atoms, pointing towards the interstitial lattice sites not only in Ruddlesden–Popper type oxides.[12,13] Analysis of the apical oxygen disorder scenario becomes thus important for a microscopic understanding of the diffusion mechanism. High-resolution neutron diffraction on single crystals is a perfect method to experimentally determine the nuclear density distribution of the respective apical oxygen atoms. Sr doping and oxygen doping are equivalent in the sense that both increase hole concentration, modifying structural and electronic ordering. Comparing both doping methods is interesting by itself, especially because the reaction temperatures are not the same, due to the fact that O doping is carried out by electrochemical reaction and thus is performed even at ambient temperature, while Sr doping definitively requires high temperatures.

The availability of single phase, high purity and large single crystals is nevertheless mandatory for detailed structure and lattice dynamics studies.

For these reasons, we investigated the growth of large and high quality single crystals, intended to perform detailed structure analysis by X-ray and neutron diffraction, and investigate changes in their lattice dynamics associated to the amount of Sr and δ.

Among the single-crystal growth techniques, the floating zone methods show several advantages, *e.g.* the absence of impurities compared to methods using crucibles, as well as the possibility of obtaining high quality single crystals of sufficiently large size for accurate structural and dynamics characterisation. Here we report on $(Nd/Pr)_{2-x}Sr_xNiO_{4+\delta}$ crystal growth conditions to obtain centimetre size, high quality single crystals by the floating zone method, and their characterization by scattering techniques (neutron and X-ray diffraction) as well as electron microscopy and thermogravimetric studies.

Experimental section

Synthesis and single crystal growth

Selected composition (x = 0.0, 0.1 and 0.5) of $RE_{2-x}Sr_xNiO_{4+\delta}$ (RE = Nd, Pr) starting materials for feed and seed rods were prepared by classical solid-state reactions at high temperature. Stoichiometric amounts of Nd_2O_3, Pr_6O_{11}, $SrCO_3$ and NiO powders (99.9% purity, Alfa Aesar) were thoroughly ground, and then heated for 12 h at 1250 °C in air. This preparation step was repeated three times with intermediate grinding and pelletizing. Nd_2O_3 was heated under dynamic vacuum at 900 °C overnight to remove any hydroxide traces, prior to the synthesis. To compensate steady evaporation of NiO during the crystal growth, an excess of NiO was added to the stoichiometric starting material; for the used growth conditions, the optimum amount was found to be a 2% molar NiO excess. Seed and feed rods for crystal growth were obtained by hydrostatic pressing of the as-synthesized NiO-enriched $(Nd/Pr)_{2-x}Sr_xNiO_{4+\delta}$ powders at 10 bars in a cylindrical latex tube of 8 mm in diameter and 150 mm in

length. Subsequent sintering at 1200 °C for 12 h allowed obtaining dense polycrystalline rods. The crystal growth was carried out using a two-mirror optical floating zone furnace (NEC SC2, Japan) equipped with two 500 W halogen lamps.[14] The growth was carried out at a speed of 2–3 mm h^{-1} with the feed and seed rods counter rotating at 35 rpm. For both compounds $(Pr/Nd)_{2-x}Sr_xNiO_{4+\delta}$ the growth process was initiated using a polycrystalline seed rod. While for $Nd_{2-x}Sr_xNiO_{4+\delta}$ (NSNO) one growth step was sufficient to obtain homogeneous cation-stoichiometric and cylindrical shaped crystals, a seed crystal from a previous growth was used for $Pr_{2-x}Sr_xNiO_{4+\delta}$ (PSNO) crystal growth. Crystal growth conditions were found to operate best when carried out in oxygen flux (pure oxygen, 99.99%).

Thermogravimetric studies

In order to determine the overall oxygen stoichiometry, thermogravimetric (TGA) measurements were carried out using a SETARAM thermo-balance applying a 5% H_2/Ar gas mixture for reduction with a heating rate of 5 °C min^{-1}. All measurements were performed on ground single crystals.

X-ray and neutron diffraction

Phase purity of all grown crystals was checked by laboratory X-ray powder diffraction with a Bruker AXS D8 Advance diffractometer using $CuK\alpha_1$ radiation. The bulk crystal quality of the as-grown single crystals was investigated by single crystal neutron diffraction using different 4-circle neutron diffractometers equipped with a point detector (5C2@LLB at the ORPHEE reactor in Saclay, France (λ = 0.83 Å), and HEiDi@MLZ at the FRM II reactor in Garching, Germany, at λ = 1.18 Å).

Electron microscopy

The crystal quality and elemental composition were checked by scanning electron microscopy (SEM) analysis using a JEOL JSM 6400 microscope, equipped with an OXFORD INCA EDS instrument for atomic recognition *via* X-ray fluorescence spectroscopy. SEM/EDS analyses were performed on a cross section (6–7 mm in diameter) of all grown crystals, after an accurate surface polishing and cleaning.

Transmission electron microscopy (TEM) was performed with a JEOL 2000 FX electron microscope, equipped with a cryogenic double-tilt (±40°) specimen stage. Specimens were prepared by grinding single crystal samples in an agate mortar in ethanol to obtain a suspension. A droplet of the suspension was then deposited on a grid covered with a carbon supported film. The electron diffraction (ED) patterns were observed by selected area diffraction (SAED).

Results and discussion

Crystal growth and quality

A series of experimental parameters need to be specifically adjusted and controlled in order to obtain cation stoichiometric $RE_2NiO_{4+\delta}$ phases. The starting composition and velocity of crystal growth at the melting point affect the stability of the molten zone during the crystal growth process. Consequently, the evaporation rate of NiO becomes a decisive parameter for the quality of the $Nd_{2-x}Sr_xNiO_{4+\delta}$ and $Pr_{2-x}Sr_xNiO_{4+\delta}$ single crystals. Evaporation of NiO during crystal growth was also observed for $La_2NiO_{4+\delta}$ crystals.[15] The polycrystalline powders used to make the rods were synthesized, adding an excess of 2% NiO to the stoichiometric ratio in order to compensate for the Ni-loss during growth. Using less than this amount resulted in a higher Nd (or Pr)/Ni ratio, leading to unstable melting and the formation of RE_xO_y intergrowth phases, while addition of higher NiO amount resulted in NiO

segregation and/or formation of Ni-rich intergrowth. As an example, NiO segregation in $Nd_2NiO_{4+\delta}$ becomes evident as shown in Fig. 1a and b, observed by SEM and confirmed by elemental analysis using energy dispersive spectroscopy (EDS) (Table 1).

Table 1 EDS analysis of the as-grown and polished $Nd_2NiO_{4+\delta}$ crystal at points 1 and 2 as shown in Fig. 1b, when the excess of NiO added to the nutrient rod was above 2% (the error on the atomic composition is of the order of 1%)

Element	Point 1 (at %)	Point 2 (at %)
Nd	31.56	0.61
Ni	15.13	55.83
O	53.31	43.57

No segregation was observed for a 2% NiO excess addition (Fig. 1c). A related problem, and more specific to $Pr_2NiO_{4+\delta}$ (PNO), concerns its decomposition into $Pr_4Ni_3O_{10-x}$ and the binary oxide PrO_y, especially in the presence of NiO, when heated above 850 °C in air.[16] Similar decompositions were already reported for $La_2NiO_{4+\delta}$ single crystals, where the epitaxial growth of $La_4Ni_3O_{10-x}$ was observed on specific lattice planes.[17] Using laboratory X-ray diffraction, we checked the phase purity of the feed rods after each preparation step and found that 12 h heating of structurally pure and polycrystalline PNO in air at 1000 °C was sufficient to clearly evidence its partial disproportionation into Pr_6O_{11} and $Pr_4Ni_3O_{10-x}$ (Fig. S1 in the ESI†). It is not clear whether this disproportionation reaction is thermodynamically or kinetically controlled as already discussed in ref. 17. We underline that the thermal stability of PNO in air depends on its synthesis conditions. While polycrystalline PNO, obtained from ground single crystals, is stable at long term (>1 week) at temperatures around 1000 °C, phases obtained by classical solid-state reactions are not. One might argue that pure PNO and cation-stoichiometric PNO, as realized during single crystal growth, are not yielded in the same quality when using classical reaction conditions, especially in terms of the presence of intergrowth phases. This suggests that PNO obtained by classic solid-state synthesis methods is supposed to contain a significant amount of intergrowth phases reported above. We note that intergrowth phases similar to the NiO segregation observed here are a well-known phenomenon for unidirectionally solidified eutectics in oxide ceramics or alloys.[18,19] Precisely adjusted cation stoichiometry, as obtained by the floating zone synthesis method for single crystals, is thus important for technological applications, as *e.g.* oxygen membranes, because any deviation from the ideal stoichiometry yields severe material limitations. In terms of overall cation stoichiometry, the presence of $NiO/Pr_4Ni_3O_{10-x}$ is, however, a critical problem for crystal growth. It required using a two-step growth, using in the second and last growth a monocrystalline rod from a previous growth. The same holds for $Nd_2NiO_{4+\delta}$.

High purity $Nd_{2-x}Sr_xNiO_{4+\delta}$ and $Pr_{2-x}Sr_xNiO_{4+\delta}$ crystals with very good crystallinity were successfully grown under O_2 atmosphere. As an example, PSNO crystals with x = 0, 0.1 and 0.5 are shown in Fig. 2. An attempt to use high-pressure argon atmosphere, as described in ref. 20, yielded crystals which disintegrated in air after some days. The length of the as-grown crystals was usually about 110 mm with a diameter of about 6 mm.

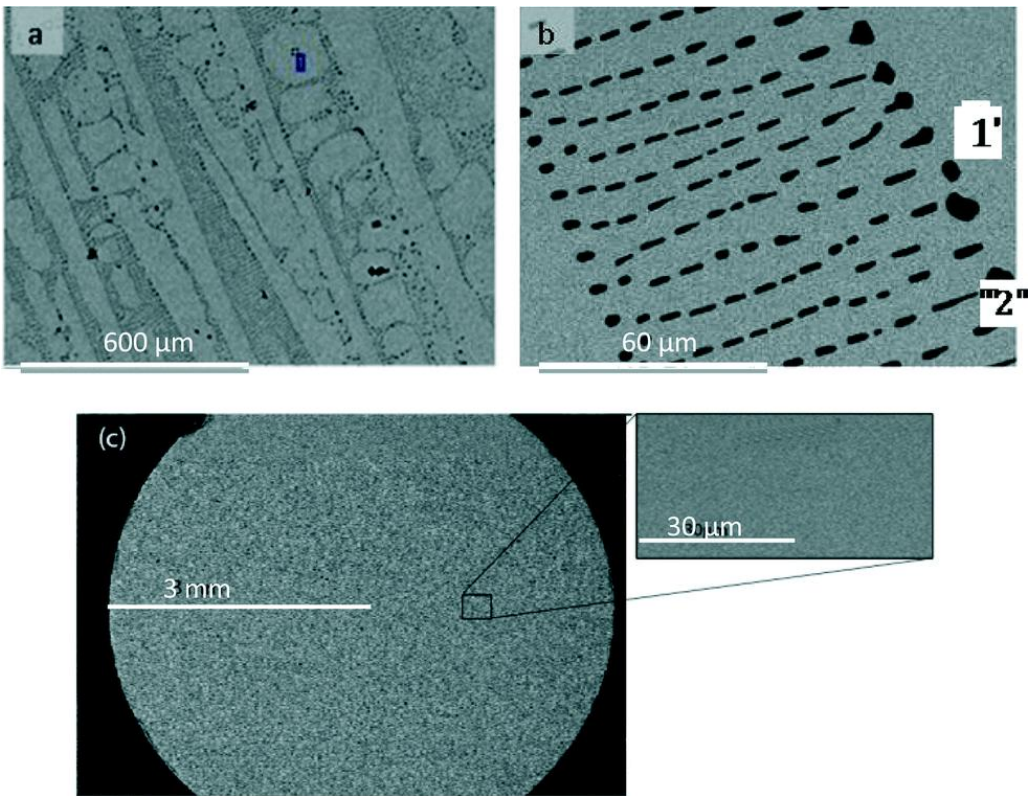

Fig. 1 (a) SEM images of the cross-section for a $Nd_2NiO_{4+\delta}$ crystal with 6 mm Ø, containing an excess of NiO higher than 2%, and (b) the zoomed view. At point no. 1, elemental analysis (see Table 1) indicates a Nd/Ni ratio of about 2 which corresponds to the chemical formula $Nd_2NiO_{4+\delta}$. At the black spots (point no. 2), the atomic percentage of Nd element is almost zero, indicating a predominant presence of NiO. In the bottom part (c) are the SEM image of the cross section and the zoomed view of the NNO single crystal when an excess of exactly 2% of NiO is added, not showing any presence of intergrowth phases.

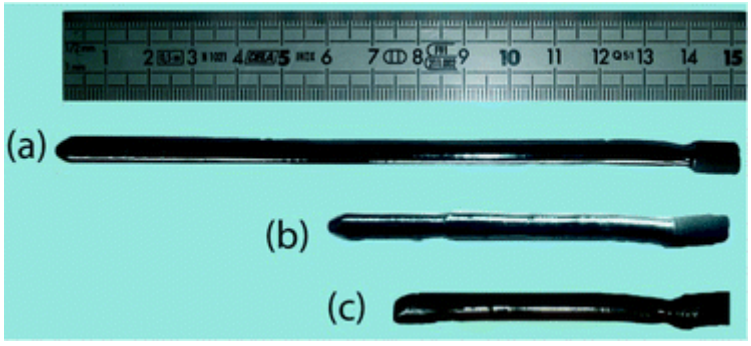

Fig. 2 Typical examples of as-grown single crystals of (a) $Pr_2NiO_{4+\delta}$; (b) $Pr_{1.9}Sr_{0.1}NiO_{4+\delta}$ and (c) $Pr_{1.5}Sr_{0.5}NiO_{4+\delta}$ obtained by the floating zone method under oxygen flow.

Phase purity of the grown single crystals was checked by X-ray powder diffraction on small sections of the as-grown single crystals that were crushed into fine powders, while PSNO crystals were all found to be homogeneous and monophasic (Fig. S2†), being orthorhombic when x = 0 or 0.1 and tetragonal when x = 0.5. NSNO crystals showed a broader distribution of the oxygen stoichiometry, as evidenced by XRD (Fig. S3 in the ESI†). After heat treatment in air at 430 °C for 3 days, all NSNO single crystals turned out to be single phase, adopting the orthorhombic *Fmmm* space group for x = 0 and x = 0.1, while their symmetry becomes tetragonal with the *I*4/*mmm* space group for x = 0.5 (see Fig. 3), as the homologue PSNO system. As a consequence, all NSNO crystals were annealed under these conditions prior to all experiments.

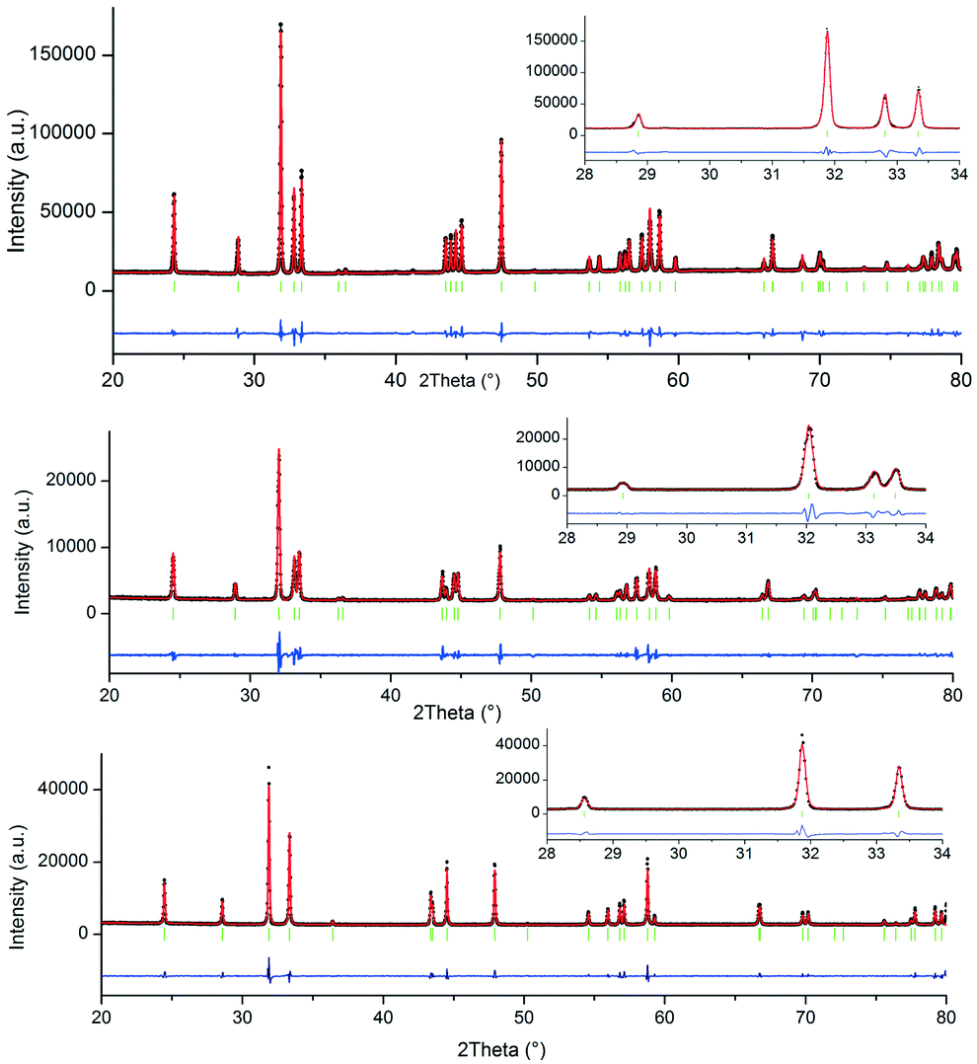

Fig. 3 X-ray diffraction patterns of crushed NSNO single crystals after annealing at 430 °C. The upper diagram was obtained for x = 0.00, the middle for x = 0.1 (both orthorhombic), while the bottom corresponds to x = 0.5 with tetragonal symmetry. We underline the excellent crystalline quality of all compounds, showing FWHM close to the resolution function of the diffractometer. Similar patterns have been obtained for PSNO crystals (Fig. S2† in the ESI).

Pattern profile refinement carried out in the profile matching mode through the Fullprof software[21] resulted in the lattice parameters reported in Table 2, which are in good agreement with the values reported elsewhere.[22,23]

Chemical composition and homogeneity of the crystals were checked using SEM coupled with EDS analysis. For this purpose, a slice of each crystal was taken perpendicular to the growth direction and polished mechanically. The crystals were found to be free of cracks or inclusions of secondary phases (Fig. 1c).

Table 2 Lattice parameters of NSNO and PSNO as obtained by a pattern profile refinement, carried out in the profile matching mode through the Fullprof software[21]

x	Space group	a (Å)	b (Å)	c (Å)
$Pr_{2-x}Sr_xNiO_{4+\delta}$				
0	*Fmmm*	5.3962(2)	5.4525(2)	12.4402(2)
0.1	*Fmmm*	5.3883(2)	5.4257(2)	12.4614(2)
0.5	*I4/mmm*	3.7837(2)	—	12.5537(2)
$Nd_{2-x}Sr_xNiO_{4+\delta}$				
0	*Fmmm*	5.3706(4)	5.4558(4)	12.3652(1)
0.1	*Fmmm*	5.3656(6)	5.4216(7)	12.3820(2)
0.5	*I4/mmm*	3.7851(3)	—	12.4715(2)

Different points throughout the cross-section of the crystal were analysed to verify the composition of the crystal. It was found that the atomic percentage of both neodymium/praseodymium and nickel remains constant over the whole cross section. For the undoped crystals, the Nd/Ni and Pr/Ni ratios are about 2 throughout the whole cross-section (see Table 3 and Fig. S4 of the ESI†), which is in agreement with the chemical formula of $Nd_2NiO_{4+\delta}$ and $Pr_2NiO_{4+\delta}$. Also, for the Sr-doped crystals, the Sr/Nd(Pr) ratios are in a good agreement with the initial stoichiometry (Table 3), indicating that there is no significant loss of strontium during the crystal growth process.

Table 3 Chemical composition, as determined by EDS, and oxygen ($4 + \delta$) content of the as-grown NSNO and PSNO crystals determined using TGA. x values are given both for nominal starting stoichiometry and from EDS measurements

Nominal starting	EDS	Oxygen content $4 + \delta$
NSNO: Nd/Sr composition		
2.0/0.0	2.0/0.0	4.23 ± 0.02
1.9/0.1	1.88(2)/0.12(2)	4.11 ± 0.02
1.5/0.5	1.47(2)/0.53(2)	4.07 ± 0.02
PSNO: Pr/Sr composition		
2.0/0.0	2.0/0.0	4.22 ± 0.02
1.9/0.1	1.89(2)/0.11(2)	4.12 ± 0.02
1.5/0.5	1.48(3)/0.52(3)	4.06 ± 0.02

The oxygen stoichiometry of the as-grown crystals was determined by TGA in reducing atmosphere (Ar + 5% H_2). The reduction curves for NSNO and PSNO (x = 0, 0.1, 0.5) are depicted in Fig. 4a and b, respectively, where the weight change is reported as a function of temperature. For $Nd_{2-x}Sr_xNiO_{4+\delta}$ crystals (Fig. 4a) with x = 0.0 and x = 0.1, it follows the characteristic two-stage reduction process.[24] For x = 0, the first oxygen loss was observed around 300 °C (350 °C for x = 0.1), corresponding to the loss of excess oxygen yielding the stoichiometric phase $Nd_{2-x}Sr_xNiO_{4.00}$. The second and larger loss, starting at around 500 °C (600 °C for x = 0.1), corresponds to the decomposition of the whole phase into $(1 - x/2)Nd_2O_3$, (x)SrO and Ni, as checked by XRD. From these assumptions, it was possible to deduce the value of δ to be 0.22 ± 0.02 for x = 0 and 0.11 ± 0.02 for x = 0.1. For composition with x = 0.5, the reduction process showed a different feature. A continuous weight loss of 0.3%, reaching the stoichiometric composition $Nd_{1.5}Sr_{0.5}NiO_{4.00}$ at around 450 °C, is observed first. A second loss of 1.5%

is further observed between 450 °C and 700 °C. This weight loss is significantly higher compared to the other compositions, indicating the formation of the oxygen deficient phase corresponding to $Nd_{1.5}Sr_{0.5}NiO_{3.71}$, similar to $Nd_{1.8}Sr_{0.2}NiO_{3.72}$, as reported in ref. 25.

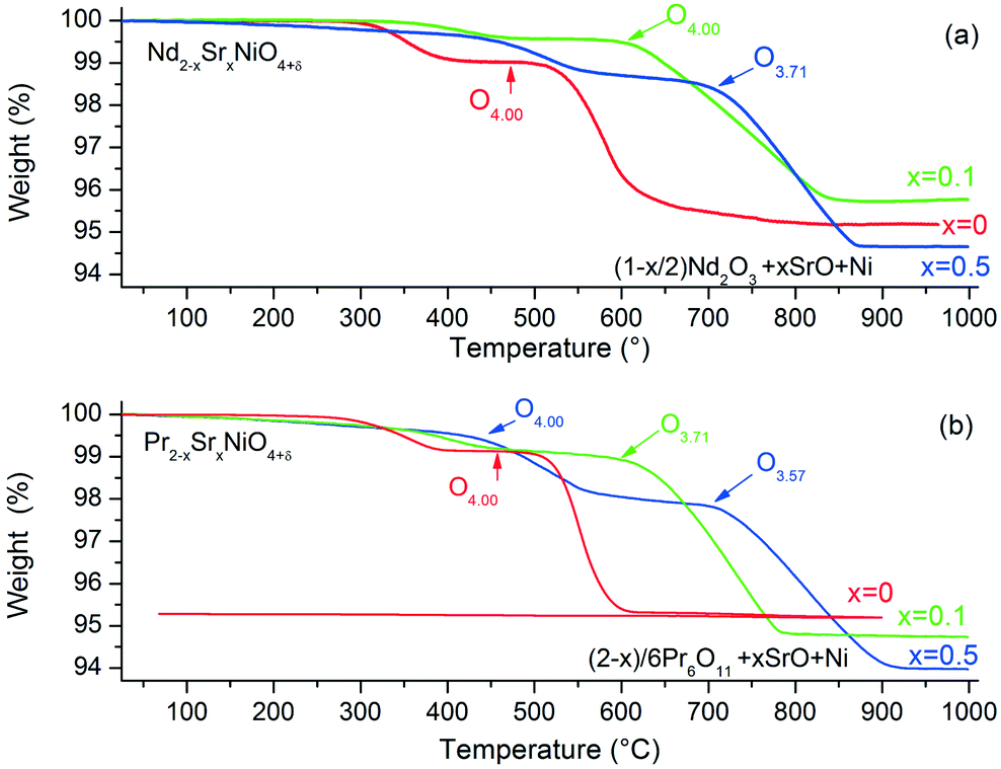

Fig. 4 TGA weight loss curve obtained in Ar/5% H_2 atmosphere with a heating rate of 5 K min^{-1} of (a) NSNO (x = 0.0, 0.1 and x = 0.5) and (b) PSNO (x = 0.0, 0.1 and x = 0.5) both obtained from ground single crystals. For $Pr_{1.5}Sr_{0.5}NiO_{4+\delta}$ the weight loss starting above 400 °C yields a new phase with an oxygen stoichiometry corresponding to $Pr_{1.5}Ni_{0.5}NiO_{3.57}$, while for the homologous Nd phase, oxygen deficiency limited to $Nd_{1.5}Sr_{0.5}NiO_{3.71}$ is obtained.

The behaviour of $Pr_{2-x}Sr_xNiO_{4+\delta}$ during reduction is analogous to its Nd homologue for x = 0, while for x = 0.1, it reaches the oxygen deficient phase $Pr_{2-x}Sr_xNiO_{3.71}$ at around 600 °C. For x = 0.5 the weight loss is significantly higher (almost 2%), suggesting the formation of a new oxygen deficient phase, corresponding to $Pr_{1.5}Sr_{0.5}NiO_{3.57}$, whose structure is presently under investigation and which is probably similar to $La_2CuO_{3.5}$ or $Nd_2CuO_{3.5}$.[26,27]

From these assumptions the oxygen content of the as-grown $(Pr/Nd)_{1.5}Sr_{0.5}NiO_{4+\delta}$ single crystal was found to be 4.06 ± 0.02.

The oxygen content of the as-grown crystals is reported in Table 3 together with the chemical composition.

Single crystal neutron diffraction

The crystalline quality of all NSNO and PSNO crystals, including possible twinning, was checked systematically by single crystal neutron diffraction. To this end, the crystals were aligned with the *c*-axis perpendicular to the diffraction plane of the diffractometer; pure transversal scans (ω scans) were carried out for characteristic reflections such as (*h*00), (*hh*0) and (00ℓ), in order to determine the related orthorhombicity and peak width.

As seen in Fig. 5 and 6, the full width at half maximum for all reflections, measured in transversal mode, is within or close to the respective instrumental resolution.[28,29] The rocking curve of *e.g.* the (006) reflection indicates the mosaicity of the as-grown crystals NSNO and PNSO to be of the order of 0.2° which is, however, increasing with the Sr content. The *ω*-scans for the (*hh*0) reflections, *i.e.* the (220) and the equivalent (−220) reflections, show a different number of twin individuals for orthorhombic Sr-free PNO and NNO crystals. For NNO, the (220) reflection was observed to split into two distinct reflections (Fig. 5b), while the (−220) profile yields only one reflection, which is in agreement with the formation of two twin domains. For x = 0.1, three contributions are obtained for (*hh*0) reflections (Fig. 5d), in agreement with the presence of 4 twin individuals overall.[30] On the other hand, PNO is twice twinned (Fig. 6b), while PSNO, with x = 0.1 (Fig. 6d), is once twinned only.

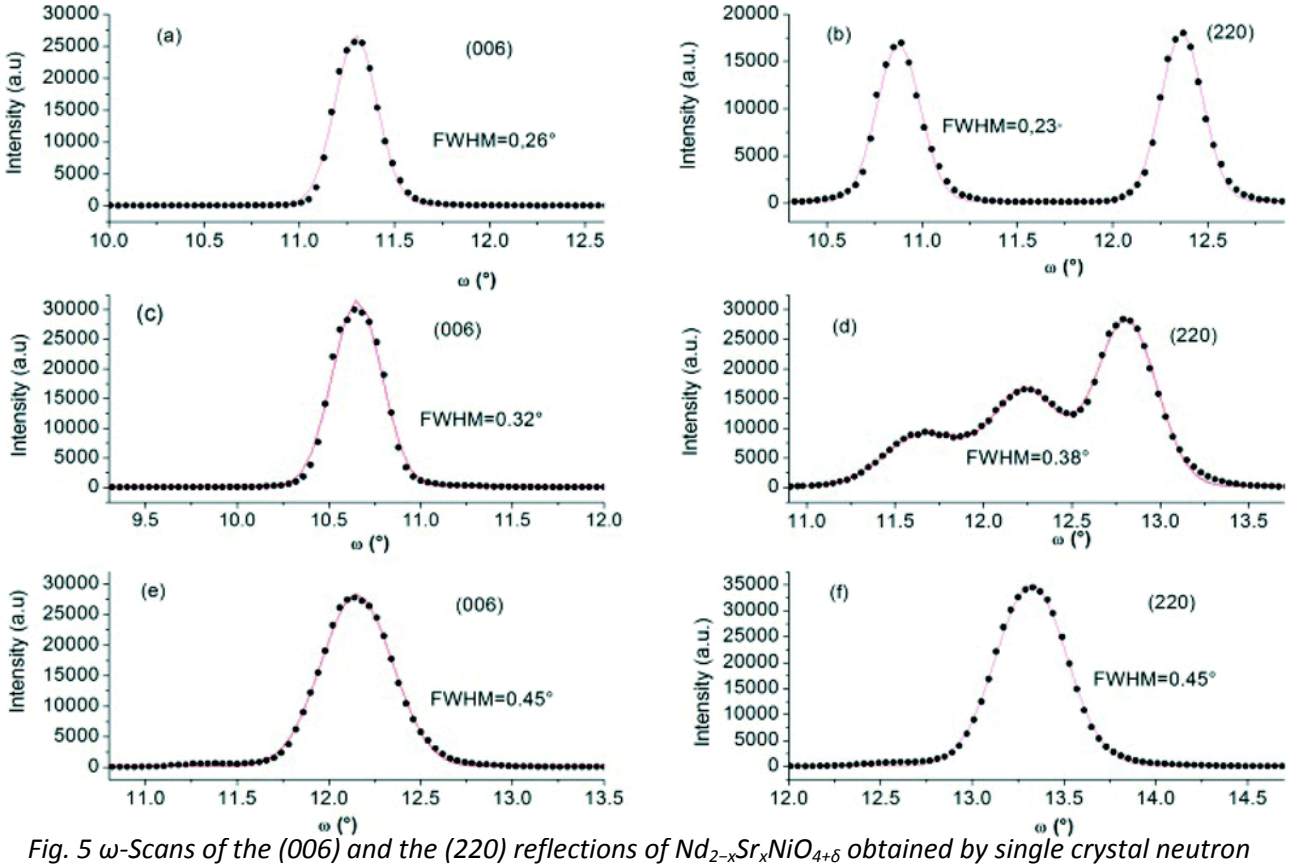

Fig. 5 ω-Scans of the (006) and the (220) reflections of $Nd_{2-x}Sr_xNiO_{4+\delta}$ obtained by single crystal neutron diffraction on 5C2@LLB in Saclay (λ = 0.83 Å). (a, b) x = 0, (c, d) x = 0.1, (e, f) x = 0.5.

For x = 0.5, no twinning is observed for both PSNO and NSNO crystals, since the symmetry is tetragonal at room temperature (Fig. 5e–f and 6e–f).

The sharp profiles of all (220) reflections indicate a homogeneous oxygen stoichiometry all over the crystal, as any inhomogeneity of δ is expected to result in significant profile broadening related to changes in a and b lattice parameters.

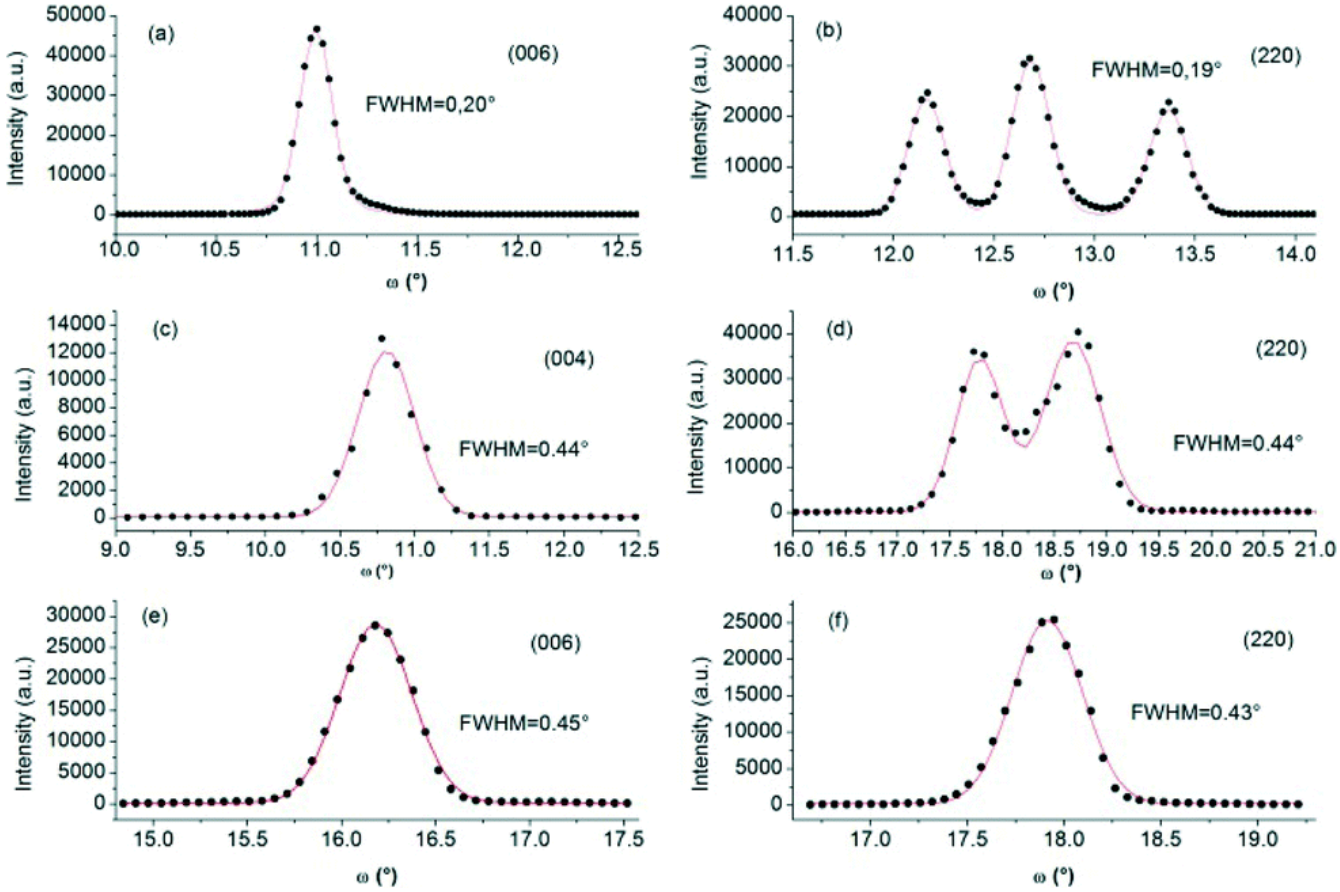

Fig. 6 ω-Scans of the (006) and (004) and the (220) reflections of $Pr_{2-x}Sr_xNiO_{4+\delta}$ obtained by single crystal neutron diffraction on 5C2@LLB in Saclay (λ = 0.83 Å, fig. 6a–b) for x = 0, and on HEIDI@FRM2 in Garching (λ = 1.18 Å) for x = 0.1 (c, d) and x = 0.5 (e, f).

Transmission electron microscopy

PNO and NNO single crystals have been studied by transmission electron microscopy in order to have a more local characterization of possible oxygen ordered phases. The second aim was to better characterize the precursor phases with respect to intergrowth phases or stacking faults. Problems related to TEM investigations may arise from changes in the stoichiometry of these non-stoichiometric oxides when studied under vacuum under reducing conditions. Nevertheless, complementary characterizations using TEM techniques like electron diffraction are essential with respect to a better characterization of local and extended defects and their importance for oxygen ion mobility.

An example of ED patterns taken along [210] from a NNO single crystal is shown in Fig. 7, where satellites between the main reflections are clearly observed. All principal spots are indexed with the orthorhombic *Fmmm* unit cell, with *a* = 5.38 Å, *b* = 5.44 Å and *c* = 12.35 Å, in agreement with those determined by X-ray diffraction.

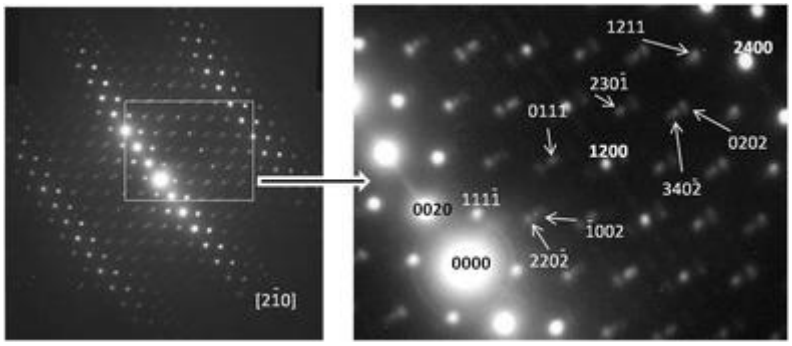

Fig. 7 Characteristic electron diffraction (ED) pattern obtained on a $Nd_2NiO_{4+\delta}$ single crystal. The spots are indexed using hklm indices, with m being related to the incommensurate modulation vector q = 0.78a* + 0.56b*. The main spots are consistent with the orthorhombic Fmmm unit cell.*

To fully understand the pattern, the introduction of an incommensurate modulation vector $q^* = 0.78a^* + 0.56b^*$ is necessary. The whole pattern can then be indexed using four *hklm* indices in a (3 + 1) dimension. In the pattern shown in Fig. 8, modulation reflections of up to order 2 are visible. In most cases, only modulation reflections of order 1 are observed as evident in Fig. 8a.

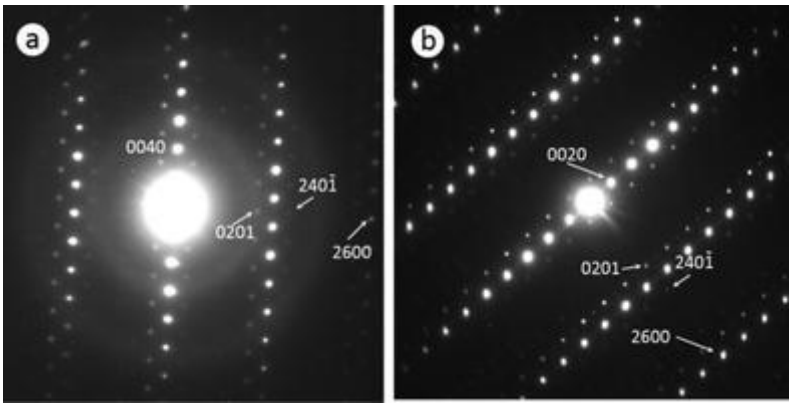

Fig. 8 Electron diffraction pattern along the same zone axis of a) $Nd_2NiO_{4+\delta}$ and b) $Pr_2NiO_{4.25}$.

Similar ED patterns have been observed in $Pr_2NiO_{4.25}$ single crystals, where main reflections have been indexed with a *Fmmm* unit cell with a = 5.39 Å, b = 5.46 Å and c = 12.44 Å, with a modulation vector $q^* = 0.73\ a^* + 0.53\ b^*$. For comparison Fig. 8b presents a typical electron diffraction pattern obtained on $Pr_2NiO_{4.25}$ with the same orientation as that related to $Nd_2NiO_{4+\delta}$.

Similar structural modulations have been already observed on nickelates[31–34] and cobaltates,[35] revealing complex oxygen interstitial ordering in the K_2NiF_4 type oxides. Determination of the present symmetry, the super space group as well the change of the wave vector as a function of Sr doping is in progress.

Most of the crystallites characterized by electron diffraction reveal for both compounds the incommensurate modulation described above. Nevertheless, patterns obtained on a limited number of crystallites presented different superstructures.

For instance, two different incommensurate patterns were obtained for $Nd_2NiO_{4+\delta}$ as presented in Fig. 9a and b. The differences are supposed to be related to small deviations in the oxygen stoichiometry, probably induced by the reducing character of the electron beam, which together with the applied vacuum conditions favour easy oxygen loss in the title compounds. Applying low temperature conditions might allow one to avoid changes in the oxygen stoichiometry and is presently under investigation.

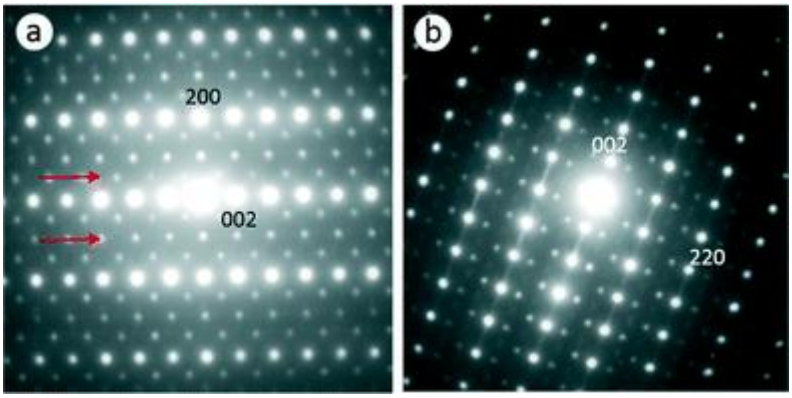

Fig. 9 Different superstructures observed on $Nd_2NiO_{4+\delta}$. The red arrows on pattern a) indicate the superstructure spots related to a complex superstructure. The weaker reflections on pattern b) arise from a 3a × 3b superstructure.

Conclusions

High quality, large size single crystals of $Nd_{2-x}Sr_xNiO_{4+\delta}$ and $Pr_{2-x}Sr_xNiO_{4+\delta}$ (x = 0.0, 0.1 and 0.5) were successfully grown with the help of a mirror furnace, using the floating zone method. The optimized growth parameters allowed obtaining large and homogeneous crystals without a significant mosaic spread and stacking faults. The high crystalline quality was also confirmed by diffraction measurements (X-rays and neutrons) as well as scanning electron microscopy coupled with elemental analysis (EDS).

The main problem to overcome for crystal growth was related to the adjustment of exact cation stoichiometry for the final crystals. Even a small deviation from the ideal cation stoichiometry, results, for both systems, in either segregation of NiO or formation of the intergrowth phase, *e.g.* $Pr_4Ni_3O_{10-x}$, while an excess of the RE metal yields Re_xO_y intergrowth phases, leading to rapid disintegration of the crystals already under ambient conditions in air. For the pure PNO and NNO crystals we noted high temperature (1000 °C) stability in air, which is by far superior compared to polycrystalline samples synthesized by classical solid state synthesis. This is an important observation especially in view of potential applications of these compounds to serve as membranes in SOFCs. Summarizing the difficulties related to deviations from the ideal cation stoichiometry and associated formation of different types of intergrowth phases, one might assume the general presence of an important concentration of intergrowth phases for conventionally prepared samples *via* solid state reaction at high temperatures. TGA analysis confirmed the insertion of extra oxygen atoms on interstitial sites, which is still valid even for higher Sr doping concentrations as is the case for $(Pr/Nd)_{2-x}Sr_xNiO_{4+\delta}$, where δ is 0.06(2), while for x = 0.1, δ is found to reach 0.12(2).

Electron diffraction revealed strong contributions of incommensurate reflections in Sr-free crystals, in addition to the stronger basic reflections. Their intensities are nevertheless significant, suggesting strong structural modulations induced by oxygen ordering. Structure analysis taking into account these incommensurate modulations is presently under way.

Acknowledgements

This research was supported by the French National Research Agency through the project FUSTOM (ANR-08-BLAN-0069). We acknowledge the use of neutron beam time on the diffractometers 5C2 at the LLB and on HEIDI at FRMII.

References

1. J. D. Jorgensen , B. Dabrowski , S. Pei , D. R. Richards and D. G. Hinks , *Phys. Rev. B: Condens. Matter Mater. Phys.*, 1989, **40** , 2187 —2199.
2. J. D. Sullivan , D. J. Buttrey , D. E. Cox and J. Hriljac , *J. Solid State Chem.*, 1991, **94** , 337 —351.
3. M. T. Fernández-Díaz , J. Rodríguez-Carvajal , J. L. Martínez , G. Fillion , F. Fernández and R. Saez-Puche , *Z. Phys. B: Condens. Matter*, 1991, **82** , 275.
4. K. Ishikawa , K. Metoki and H. Miyamoto , *J. Solid State Chem.*, 2009, **182** , 2096 —2103.
5. M. T. Fernández-Díaz , J. L. Martínez and J. Rodríguez-Carvajal , *Solid State Ionics*, 1993, **63–65** , 902 —906.
6. C. C. Homes , J. M. Tranquada and D. J. Buttrey , *Phys. Rev. B: Condens. Matter Mater. Phys.*, 2007, **75** , 045128.
7. S. Anissimova , D. Parshall , G. D. Gu , K. Marty , M. D. Lumsden , S. Chi , J. A. Fernandez-Baca , D. L. Abernathy , D. Lamago , J. M. Tranquada and D. Reznik , *Nat. Commun.*, 2014, **5** , 3467.
8. E. Boehm , J. M. Bassat , P. Dordor , F. Mauvy , J. C. Grenier and P. Stevens , *Solid State Ionics*, 2005, **176** , 2717 —2725.
9. C. Ferchaud , J.-C. Grenier , Y. Zhang-Steenwinkel , M. M. A. van Tuel , F. P. F. van Berkel and J.-M. Bassat , *J. Power Sources*, 2011, **196** , 1872 —1879.
10. F. Chauveau , J. Mougin , F. Mauvy , J.-M. Bassat and J.-C. Grenier , *Int. J. Hydrogen Energy*, 2011, **36** , 7785 —7790.
11. A. Villesuzanne , W. Paulus , A. Cousson , S. Hosoya , L. Le Dreau , O. Hernandez , C. Prestipino , M. I. Houchati and J. Schefer , *J. Solid State Electrochem.*, 2011, **15** , 357 —366.
12. A. Perrichon , A. Piovano , M. Boehm , M. Zbiri , M. Johnson , H. Schober , M. Ceretti and W. Paulus , *J. Phys. Chem. C*, 2015, **119** , 1557 —1564.
13. X. Li and N. A. Benedek , *Chem. Mater.*, 2015, **27** , 2647 —2652.
14. M. Ceretti , A. Piovano , A. Cousson , T. Berthier , M. Meven , G. Agostini , J. Schefer , O. Hernandez , C. Lamberti and W. Paulus , *CrystEngComm*, 2012, **14** , 5771 —5776.
15. W.-J. Jang , K. Imai , M. Hasegawa and H. Takei , *J. Cryst. Growth*, 1995, **152** , 158.
16. P. Odier , C. Allançon and J. M. Bassat , *J. Solid State Chem.*, 2000, **153** , 381 —385.
17. N. Gauquelin , T. Weirich , M. Ceretti , W. Paulus and M. Schroeder , *Monatsh. Chem.*, 2009, **140** , 1095 —1102.
18. H. Laroui , M. Dechamps , G. Dhalenne and A. Revcolevschi , *J. Mater. Sci.*, 1989, **24** , 562 —568.
19. Z. Xu and G. Liang , *Metall. Mater. Trans. A*, 2006, **37** , 3665 —3675.
20. D. Prabhakaran , A. T. Boothroyd and D. Gonzalez , *J. Mater. Sci.: Mater. Electron.*, 2003, **14** , 583 —586.
21. J.Rodríguez-Carvajal, IUCr Newsletter, 2001, vol. 26, pp. 12–19, The complete FULLPROF suite can be obtained from: http://www.ill.eu/sites/fullprof/index.html
22. K. Ishizaka , Y. Taguchi , R. Kajimoto , H. Yoshizawa and Y. Tokura , *Phys. Rev. B: Condens. Matter Mater. Phys.*, 2003, **67** , 184418.
23. S. C. Chen , K. V. Ramanujachary and M. Greenblatt , *J. Solid State Chem.*, 1993, **105** , 444 —457.
24. H. Zhao , F. Mauvy , C. Lalanne , J. M. Bassat , S. Fourcade and J. C. Grenier , *Solid State Ionics*, 2008, **179** , 2000 —2005.
25. M. Medarde , J. Rodríguez-Carvajal , M. Vallet-Regí , J. González-Calbet and J. Alonso , *Phys. Rev. B: Condens. Matter Mater. Phys.*, 1994, **49** , 8591 —8599.
26. M. I. Houchati , M. Ceretti , C. Ritter and W. Paulus , *Chem. Mater.*, 2012, **24** , 3811 —3815.
27. D. R. Pederzolli and J. P. Attfield , *J. Solid State Chem.*, 1998, **136** , 137 —140.
28. 5C2: Hot Neutron Four-Circle Diffractometer at LLB., Technical data can be found at http://www-llb.cea.fr/en/fr-en/spectro/5c2/5c2.html
29. M. Meven , V. Hutanu and G. Heger , *Neutron News*, 2007, **18** , 19 —21.
30. W. Paulus , A. Cousson , G. Dhalenne , J. Berthon , A. Revcolevschi , S. Hosoya , W. Treutmann , G. Heger and R. Le Toquin , *Solid State Sci.*, 2002, **4** , 565 —573.

31. J. M. Tranquada , J. E. Lorenzo , D. J. Buttrey and V. Sachan , *Phys. Rev. B: Condens. Matter Mater. Phys.*, 1995, **52** , 3581 —3595.

32. C. H. Chen , S. W. Cheong and A. S. Cooper , *Phys. Rev. Lett.*, 1993, **71** , 2461 —2464.

33. L. C. Otero-Diaz , A. R. Landa , F. Fernandez , R. Saez-Puche , R. Withers and B. G. Hyde , *J. Solid State Chem.*, 1992, **97** , 443 —451.

34. J. M. Tranquada , D. J. Buttrey , V. Sachan and J. E. Lorenzo , *Phys. Rev. Lett.*, 1994, **73** , 1003 —1006.

35. L. Le Dréau , C. Prestipino , O. Hernandez , J. Schefer , G. Vaughan , S. Paofai , J. M. Perez-Mato , S. Hosoya and W. Paulus , *Inorg. Chem.*, 2012, **51** , 9789 —9798.